Predictive Duty Cycle Control With Reversible Vector Selection for Three-Phase AC/DC Converters

Xiaolong Shi, *Student Member, IEEE*, Jianguo Zhu, *Senior Member, IEEE*, Li Li, Dylan Dah-Chuan Lu, *Senior Member, IEEE*, Jianwei Zhang, and Haitao Yang, *Student Member, IEEE*

***Abstract*—The conventional predictive duty cycle control (CPDCC) of three-phase full-bridge ac/dc converters selects adjacent nonzero vector pair based on the grid-voltage vector location, then the duration for each vector is calculated. Though the vector selection method is quite simple, it has a significant disadvantage that the values of calculated durations could be frequently less than zero due to nonoptimal vector selection, which results in high current harmonics and power notches. It could be improved with improved predictive duty cycle control (IPDCC) by reselecting the nonzero vector pair when negative duration exists; however, the whole vector selection and calculation procedure are repeated. By theoretical verification that the power variation rates of reversible vector pair are symmetrical with respect to that of zero vector, this paper proposes the reversible predictive duty cycle control (RPDCC) simply by replacing the original vector with its opposite vector and the recalculation of vector duration is eliminated compared with IPDCC. Thus, the calculation effort is almost not increased compared with CPDCC while system performance is significantly improved. The proposed control is theoretically derived and verified with the simulation and experimental results showing that RPDCC has better steady and dynamic performance than CPDCC and IPDCC methods.**

***Index Terms*—AC/DC converter, duty cycle control, predictive control, pulsewidth-modulated control, time duration.**

I. Introduction

THE three-phase full-bridge ac/dc converter is an attractive power electronic interface that has various applications, such as integration of distributed generations, electrical machine driving, voltage source converter transmission, active power filter, and active front-end rectifier [1], [2] due to the merits such as four quadrant power flow, input power factor correction, sinusoidal currents with low harmonic distortion, flexible dc-link voltage adjustment, and relatively low dc filter capacitance compared with uncontrolled ac/dc converters [3]–[5]. Thus, many

Manuscript received September 13, 2017; revised January 16, 2018 and April 14, 2018; accepted July 10, 2018. Date of publication July 24, 2018; date of current version March 29, 2019. Recommended for publication by Associate Editor M. Ordonez. *(Corresponding author: Xiaolong Shi.)*

X. Shi, L. Li, D. Lu, J. Zhang, and H. Yang are with the School of Electrical and Data Engineering, University of Technology Sydney, Ultimo, NSW 2007, Australia (e-mail:

in negative durations. In real control systems, it needs the compensation measure that the action time is forced to zero whenever a negative value is obtained, resulting in performance deterioration such as significant power notches and current spikes. To solve this issue, some methods have been proposed [36]–[40]. In [36], a model predictive cost function based optimal voltage vector selection is developed, and global optimal voltage vectors are selected by means of cost function minimization, which abandons using sector information and sacrifices simplicity of vector selection. In [37] and [38], the reason of negative duration with CPDCC method is analyzed and an improved predictive duty cycle control (IPDCC) with complementary vector sequence table is proposed based on the summarized characteristics of power variation rates by case study. The active voltage vectors are reselected based on an additional vector sequence table whenever negative time values appear. Then, the duration time needs to be recalculated with power slope recalculation of the reselected vectors. Thus, the complexity and calculation burden increase obviously as vector selection and duration calculation are repeated whenever there exists negative duration. Besides, it is found that the negative durations of dual nonzero vectors are not just related to the nonoptimal vector selection but with external factors, such as instantaneous power error and sampling frequency, which are ignored and not solved completely with IPDCC, as well. The authors in [39] and [40] propose an improved predictive DPC method without sector information and voltage vector selection; however, the equivalent reconstruction of switch signals is needed and the calculation of duration is complex. Some model predictive cost function based vector selection schemes are applied in [41]–[45]; however, these methods require the cost function to calculate the best vectors, which is not as intuitive as the sector information based method, and the negative duration issue still exists though not significant. Detailed comparisons of the cost function and sector information based vector selection schemes have been conducted in X. Shi's thesis [46].

This paper proposes a reversible vector selection based predictive duty cycle control (RPDCC) by first discovering and taking advantage of the fact that the power slope of opposite vector pair is symmetric with respect to the power slope of zero vector. Thus, the reverse vector could be applied to replace the original nonzero vector whenever it has negative duration, and its duration is just the absolute value of the negative duration. As the duration of zero vector with new sequence also meets the boundary condition, it can be directly derived without recalculation. Thus, there is no need to recalculate the power slopes and the durations as the IPDCC method, which reduces the control complexity obviously. Besides, comprehensive analyses about the reasoning of negative duration and more unsolved issues of the IPDCC are discussed. The superior performance of the RPDCC is verified by the simulation results and experimental results.

II. Modeling of Three-Phase Converter

Fig. 1(a) illustrates the topology of a two-level three-phase ac/dc converter. Fig. 1(b) shows the voltage space vectors. The

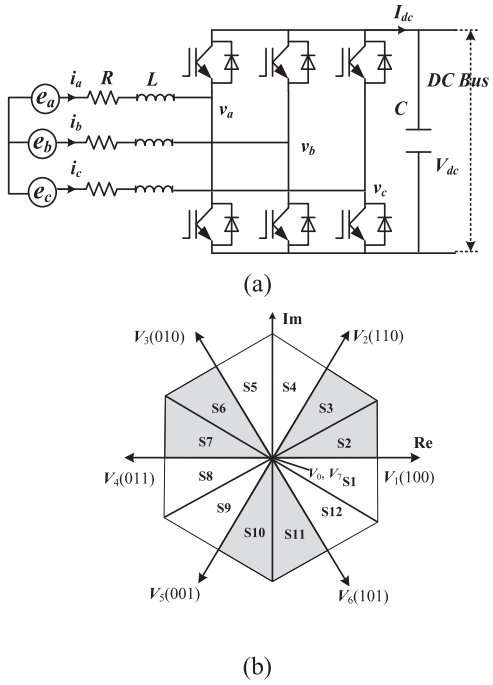

Fig. 1. (a) AC/DC three-phase converter structure. (b) Voltage space vectors.

three-phase full bridge unit is connected to the main grid via a choke consisting of three series-connected inductors *L* and resistors *R*, where e_a, e_b, and e_c are the three-phase ac source voltages, v_a, v_b and v_c are the ac terminal voltages of the three-phase bridge, and i_a, i_b, and i_c are the three-phase currents. At the dc side, a dc load or a dc bus is connected.

In the stationary reference frame, the ac source voltage vector and current vector in the $\alpha\beta$-coordinate system can be calculated by following transformation:

$$e_{\alpha\beta} = \begin{bmatrix} e_\alpha \\ e_\beta \end{bmatrix} = \frac{2}{3}\begin{bmatrix} 1 & -1/2 & -1/2 \\ 0 & \sqrt{3/2} & -\sqrt{3/2} \end{bmatrix}\begin{bmatrix} e_a \\ e_b \\ e_c \end{bmatrix} \quad (1)$$

$$i_{\alpha\beta} = \begin{bmatrix} i_\alpha \\ i_\beta \end{bmatrix} = \frac{2}{3}\begin{bmatrix} 1 & -1/2 & -1/2 \\ 0 & \sqrt{3/2} & -\sqrt{3/2} \end{bmatrix}\begin{bmatrix} i_a \\ i_b \\ i_c \end{bmatrix}. \quad (2)$$

In a balanced three-phase system, the line currents can be calculated in the stationary reference frame as follows:

$$e_{\alpha\beta} = L\frac{di_{a\beta}}{dt} + Ri_{a\beta} + v_{\alpha\beta} \quad (3)$$

where $e_{\alpha\beta}$, $v_{\alpha\beta}$, and $i_{\alpha\beta}$ are the input source voltage vector, three-phase converter input voltage vector, and line current vector, respectively. The active and reactive powers exchanged with the grid can be calculated as

$$\begin{bmatrix} P \\ Q \end{bmatrix} = \frac{3}{2}\begin{bmatrix} e_\alpha & e_\beta \\ e_\beta & -e_\alpha \end{bmatrix}\begin{bmatrix} i_\alpha \\ i_\beta \end{bmatrix}. \quad (4)$$

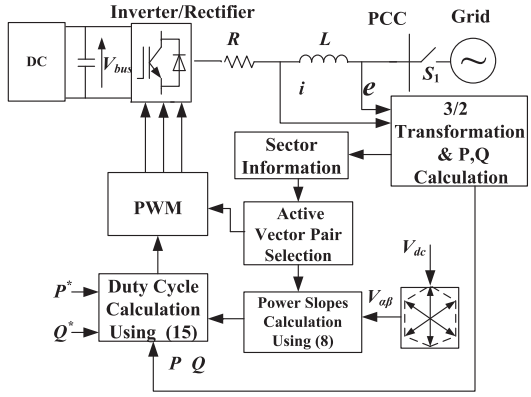

Fig. 2. Schematic diagram of CPDCC for the three-phase ac/dc converter.

TABLE I
CONVENTIONAL VOLTAGE-VECTORS' SEQUENCES FOR CPDCC [34]

Vector Sequence	Sector number (S_n)											
	S_1	S_2	S_3	S_4	S_5	S_6	S_7	S_8	S_9	S_{10}	S_{11}	S_{12}
V_{n1}	V_1	V_1	V_2	V_2	V_3	V_3	V_4	V_4	V_5	V_5	V_6	V_6
V_{n2}	V_6	V_2	V_1	V_3	V_2	V_4	V_3	V_5	V_4	V_6	V_5	V_1
V_{z0}	V_7	V_7	V_0	V_0	V_7	V_7	V_0	V_0	V_7	V_7	V_0	V_0

III. CONVENTIONAL PREDICTIVE DUTY-CYCLE-CONTROL

The CPDCC proposed in [34] is discussed in this part, as shown in Fig. 2. The selection of two active voltage vectors is strictly based on the sector information, namely the grid-voltage vector location, and the sequences are shown in Table I. Then, the duration calculation is based on the corresponding power slopes of selected nonzero vector pair and zero vector.

The differential equation of active and reactive powers can be derived from (3) and (4) as

$$\frac{d}{dt}\begin{bmatrix}P\\Q\end{bmatrix}=\frac{3}{2}\left(i_\alpha\frac{d}{dt}\begin{bmatrix}e_\alpha\\e_\beta\end{bmatrix}+\frac{di_\alpha}{dt}\begin{bmatrix}e_\alpha\\e_\beta\end{bmatrix}+i_\beta\frac{d}{dt}\begin{bmatrix}e_\beta\\-e_\alpha\end{bmatrix}+\frac{di_\beta}{dt}\begin{bmatrix}e_\beta\\-e_\alpha\end{bmatrix}\right). \tag{5}$$

For the sinusoidal and balanced three-phase line voltage

$$\bar{e}=e_\alpha+je_\beta=|\bar{e}|e^{j\omega t}. \tag{6}$$

From (6), the following expression can be deduced as

$$\frac{d}{dt}\begin{bmatrix}e_\alpha\\e_\beta\end{bmatrix}=\omega\cdot\begin{bmatrix}-e_\beta\\e_\alpha\end{bmatrix}. \tag{7}$$

Supposing $\bar{e}$ lies in a sector with two nonzero vectors V_{n1}, V_{n2} and one zero vector V_{z0}, where n_1, $n_2\in\{1,\dots 6\}$, and z_0 $\{0, 7\}$, the instantaneous active and reactive powers can be derived by substituting (1) and (7) into (5) as

$$\begin{cases}\frac{dP_i}{dt}=-\frac{R}{L}P-\omega Q+\frac{3}{2L}|\bar{e}|^2-\frac{3}{2L}\mathrm{Re}\left(\bar{e}\bar{V}_i^*\right)\\ \frac{dQ_i}{dt}=-\frac{R}{L}Q+\omega P-\frac{3}{2L}\mathrm{Im}\left(\bar{e}\bar{V}_i^*\right) & i=\{n_1,n_2,z_0\}\\ \delta_{pi}=\frac{dP_i}{dt}\quad \delta_{qi}=\frac{dQ_i}{dt}\end{cases} \tag{8}$$

where δ_{pi} and δ_{qi} are the active and reactive power slopes of each voltage space vector and $\bar{V}_i$ represents the voltage space vector selected in vector sequence. For corresponding selected voltage space vector, $V_{i\alpha}$ and $V_{i\beta}$ are calculated as follows:

$$\begin{bmatrix}V_{i\alpha}\\V_{i\beta}\end{bmatrix}=\frac{2}{3}V_{dc}\begin{bmatrix}S_{ia}-\frac{1}{2}(S_{ib}+S_{ic})\\\frac{\sqrt{3}}{2}(S_{ib}-S_{ic})\end{bmatrix} \tag{9}$$

where S_{ia}, S_{ib}, and S_{ic} are the switching states of the converter.

If the tracking error of the dc-bus voltage is assumed constant over two successive sampling periods, the instantaneous active power at the next sampling instant $(k+1)$ can be estimated using a linear extrapolation. Thus, at the end of sampling period Δt, the predicted active and reactive powers for each converter switching state can be expressed as

$$\begin{bmatrix}P_i(t+\Delta t)\\Q_i(t+\Delta t)\end{bmatrix}=\Delta t\left(-\frac{R}{L}\begin{bmatrix}P_i(t)\\Q_i(t)\end{bmatrix}+\omega\begin{bmatrix}-Q_i(t)\\P_i(t)\end{bmatrix}\right)+\begin{bmatrix}P_i(t)\\Q_i(t)\end{bmatrix}+\frac{3\Delta t}{2L}\begin{bmatrix}\left(|\bar{e}|^2-\mathrm{Re}\left(\bar{e}\bar{V}_i^*\right)\right)\\-\mathrm{Im}\left(\bar{e}\bar{V}_i^*\right)\end{bmatrix}. \tag{10}$$

For CPDCC, two adjacent nonzero vectors are selected according to the sector information and Table I. Assuming the power slopes are constant for a small sampling period, the powers at the end of the sampling period can be predicted as

$$\begin{cases}P^{k+1}=P^k+2(\delta_{pn1}t_1+\delta_{pn2}t_2+\delta_{pz0}t_0)\\ Q^{k+1}=Q^k+2(\delta_{qn1}t_1+\delta_{qn2}t_2+\delta_{qz0}t_0)\end{cases} \tag{11}$$

where δ_{pn1}, δ_{pn2}, and δ_{pz0} are the active power slopes of two adjacent nonzero voltage vectors V_{n1}, V_{n2} and one zero voltage vector, respectively, δ_{qn1}, δ_{qn2}, and δ_{qz0} are the reactive power slopes, respectively, and t_1, t_2, and t_0 are the corresponding durations of two adjacent nonzero voltage vectors and zero vector, respectively, which should satisfy the boundary condition $t_1+t_2+t_0=T_s/2$. Then according to (12), the error between predicted value and the reference can be calculated as

$$\begin{cases}P_{err}=P^*-\left[P^k+2(\delta_{pn1}t_1+\delta_{pn2}t_2+\delta_{pz0}t_0)\right]\\ Q_{err}=Q^*-\left[Q^k+2(\delta_{qn1}t_1+\delta_{qn2}t_2+\delta_{qz0}t_0)\right]\end{cases} \tag{12}$$

where P^* is the active power reference and Q^* is the reactive power reference. Then, the least-square optimization is utilized for duration calculation to minimize the power errors as

$$J=P_{err}^2+Q_{err}^2 \tag{13}$$

$$\begin{cases}\frac{\partial J}{\partial t_1}=0\\ \frac{\partial J}{\partial t_2}=0.\end{cases} \tag{14}$$

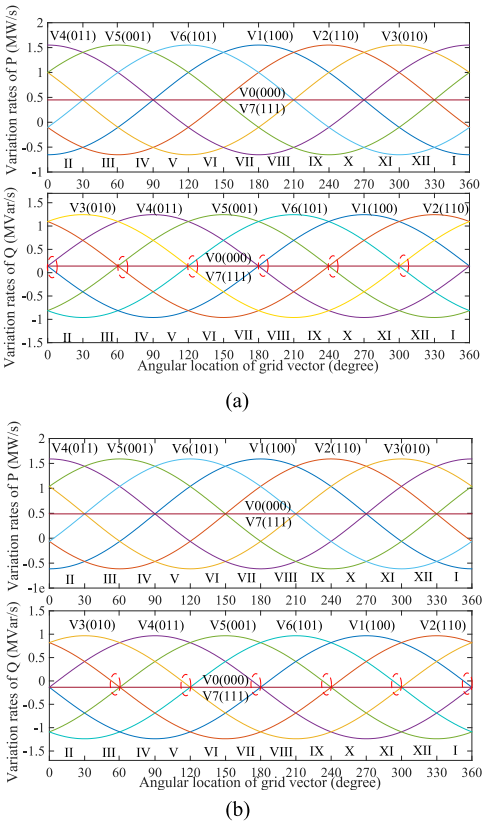

Fig. 3. Active and reactive power variation rates by using each converter voltage vector throughout 12 different sectors. (a) $P = 450$ W, $Q = 0$ Var. (b) $P = -350$ W, $Q = 200$ Var.

Finally, the optimal application durations can be obtained as follows:

$$\begin{cases} t_1 = \left[(P^* - P^k)(\delta_{qn2} - \delta_{qz0}) + (Q^* - Q^k)(\delta_{pz0} - \delta_{pn2})\right]/2m \\ \quad + T_s(\delta_{pn2}\delta_{qz0} - \delta_{pz0}\delta_{qn2})/2m \\ t_2 = \left[(P^* - P^k)(\delta_{qz0} - \delta_{qn1}) + (Q^* - Q^k)(\delta_{pn1} - \delta_{pz0})\right]/2m \\ \quad + T_s(\delta_{qn1}\delta_{pz0} - \delta_{qz0}\delta_{pn1})/2m \\ t_0 = T_s/2 - t_1 - t_2 \end{cases} \tag{15}$$

where

$$m = (\delta_{qn2} - \delta_{qz0})\delta_{pn1} + (\delta_{qz0} - \delta_{qn1})\delta_{pn2} + (\delta_{qn1} - \delta_{qn2})\delta_{pz0}. \tag{16}$$

Once t_1, t_2, and t_0 are calculated, switch duty cycles can be obtained and switching signals are generated with symmetrical $3 + 3$ voltage-vectors' sequence. However, the negative duration issue can be serious, which will be discussed next.

IV. Discussion on Reasoning of Negative Duration Issue and Current Improved Scheme [38]

To analyze the reasoning of negative duration issue, the power slope of each vector with the parameters as in Table IV is illustrated. Fig. 3(a) and (b) depicts the variation rates of instantaneous active/reactive powers using each vector throughout the

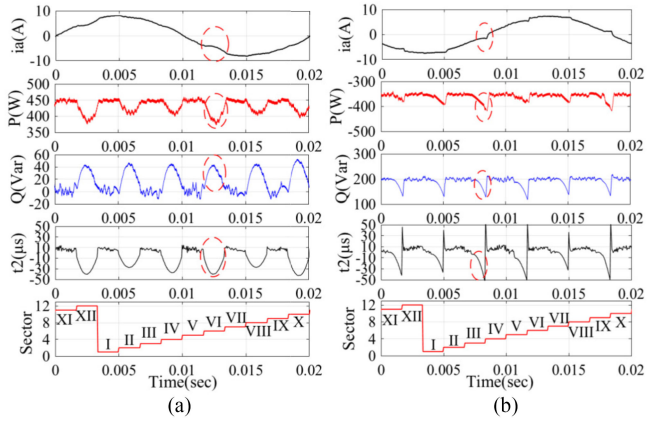

Fig. 4. Detailed system responses under various conditions. (a) $P = 450$ W, $Q = 0$ Var. (b) $P = -350$ W, $Q = 200$ Var.

12 sectors under the conditions of $P = 450$ W, $Q = 0$ Var and $P = -350$ W, $Q = 200$ Var, respectively. Taking sector VI in Fig. 3(a) as an example, V_3, V_4, and V_7 are selected according to sequence Table I. Without regard to instantaneous large power error, the instantaneous active power can be regulated properly since though V_3 and V_4 keep the active power decreased during the whole sector, V_7 could produce positive active power variation during the whole sector VI. In comparison, during the initial part of sector VI, the three selected voltage vectors all produce positive reactive power variation rate. Thus, the instantaneous reactive power cannot be controlled precisely with the positive values of predicted durations. As a result, a negative duration might be generated to meet the instantaneous reactive power regulation according to (12). The same phenomenon can be observed in the other even-numbered sectors as indicated with the dotted circle in Fig. 3(a). The detailed system responses are illustrated in Fig. 4(a); due to the negative duration at the beginning of the even-numbered sectors, the reactive power throughout the whole sector VI is out of control, resulting in significant power notches and current spikes in the even-numbered sectors. Similarly, as indicated with the dotted circle in Fig. 3(b), the reactive power cannot be precisely controlled and results in negative durations. The detailed system responses are illustrated in Fig. 4(b) and similar phenomenon can be observed in the latter part of the odd-numbered sectors.

Thus, the negative duration is mainly caused by the internal factor namely nonoptimal vector selection, and the negative duration occurrence would be more frequent while δ_{qz0} is away from 0, since the dotted circle parts would enlarge as can be easily speculated from Fig. 3 due to the symmetrical features. By (8), δ_{qz0} is related to the system parameter R, L, ω and operating condition of P and Q.

Meanwhile, the external factors such as instantaneous large power error and control period limit should be considered. For instance, when there is a reference change of active or reactive power, the instant power error of P_{err} or Q_{err} increases significantly. Thus, the solved duration for each vector by (15) for power error minimization could be negative or over $T_s/2$ due to the limited value of variation rates. Also, with higher sampling frequency, it is more difficult to mitigate the power

TABLE II
COMPLEMENTARY VOLTAGE-VECTORS' SEQUENCE OF IPDCC [38]

Vector Sequence	Sector number (S_n)											
	S_1	S_2	S_3	S_4	S_5	S_6	S_7	S_8	S_9	S_{10}	S_{11}	S_{12}
V_{n1}	V_1	V_1	V_2	V_2	V_3	V_3	V_4	V_4	V_5	V_5	V_6	V_6
V_{n2}	V_2	V_6	V_3	V_1	V_4	V_2	V_5	V_3	V_6	V_4	V_1	V_5
V_{z0}	V_7	V_7	V_0	V_0	V_7	V_7	V_0	V_0	V_7	V_7	V_0	V_0

error in one control period and the negative duration issue would be more apparent. In summary, the negative duration issue of least-square optimization based method not only results from nonoptimal vector selection in some sector parts, which is the inherent demerit of sector information based vector selection method due to fixed vector sequences, but also is generally from external factors that cannot be avoided by optimal vector pair selection.

To solve the nonoptimal vector selection, the IPDCC is proposed in [38] with an additional vector sequence table as Table II when the calculated duration is negative with the vector sequence in Table I. After the reselection of nonzero vectors, the corresponding power slopes need to be recalculated with (8), and then the optimal durations are recalculated using (15), which means the whole control procedure is almost repeated. It is no doubt that the negative duration caused by non-optimal vector selection could be improved, while the hardware system with higher computing capacity might be required since the whole control procedure is almost repeated.

Besides, the proposal of IPDCC is merely based on several case studies of power slopes related with active power flow direction, reactive power outputs and vector sequence, then the characteristics of active and reactive power variation rates in odd and even sectors are summarized, which are used to propose the additional sequence table mainly for steady states. The influence of external factors on negative duration issue is not considered, also it may lack of the theoretical verification for wide applications to solve the negative duration issue. For instance, only the negative value of t_2 is considered with IPDCC; though t_1 is positive in most cases, the negative value of t_1 still exists since the appearance of negative duration is not only related to the internal factor but also has a significant relation with external factors as discussed above. Besides, the recalculated duration after vector reselection cannot ensure to be positive, especially during dynamic-states with large power error. However, the discussion and solution on these issues are ignored, and the sequence of V_{n1} with IPDCC remains unchanged as that of CPDCC, which lack adjustment flexibility. Therefore, the control performance improvement is hindered. Thus, the negative duration issue is not solved fundamentally; it needs a totally different path to solve this issue.

V. REVERSIBLE VECTOR SELECTION BASED PREDICTIVE DUTY CYCLE CONTROL

The RPDCC method is proposed to solve the issue of negative duration with consideration of negative duration of both V_{n1} and V_{n2} while eliminating the duration recalculation. When the calculated duration is negative for a nonzero vector with CPDCC, the reverse vector is selected and the absolute value of calculated negative duration can be applied directly without recalculation. Besides, the duration of zero-vector meets the boundary condition $t_1 + t_2 + t_0 = T_s/2$ as well. Thus, the principle is very simple in calculation and easy to implement. Theoretical analyses of the proposal are presented next.

A. Theoretical Analysis

It can be concluded from (9) that

$$\begin{cases} V_{0\alpha} = V_{0\beta} = V_{7\alpha} = V_{7\beta} = 0 \\ V_{1\alpha} = -V_{4\alpha}, \quad V_{1\beta} = -V_{4\beta} \\ V_{2\alpha} = -V_{5\alpha}, \quad V_{2\beta} = -V_{5\beta} \\ V_{3\alpha} = -V_{6\alpha}, \quad V_{3\beta} = -V_{6\beta}. \end{cases} \tag{17}$$

Substituting (17) into (8), the power slope of zero vector can be derived as follows:

$$\begin{cases} \delta_{p0} = \delta_{p7} = -\frac{R}{L}P - \omega Q + \frac{3}{2L}|\bar{e}|^2 \\ \delta_{q0} = \delta_{q7} = -\frac{R}{L}Q + \omega P. \end{cases} \tag{18}$$

Taking V_1 and the reverse V_4 vector as an example, the power slope relations with zero vector can be derived

$$\begin{cases} \delta_{p1} = \delta_{p0} - \frac{3}{2L}\mathrm{Re}\left(\bar{e}\bar{V}_1^*\right) \\ \delta_{p4} = \delta_{p0} - \frac{3}{2L}\mathrm{Re}\left(\bar{e}\bar{V}_4^*\right) \\ \delta_{p1} + \delta_{p4} = 2\delta_{p0}. \end{cases} \tag{19}$$

Similarly, for nonzero vectors, relations between the original vector and its opposite vector can be derived as follows

$$\begin{cases} \delta_{p1} = 2\delta_{p0} - \delta_{p4}, \quad \delta_{q1} = 2\delta_{q0} - \delta_{q4} \\ \delta_{p2} = 2\delta_{p0} - \delta_{p5}, \quad \delta_{q2} = 2\delta_{q0} - \delta_{q5} \\ \delta_{p3} = 2\delta_{p0} - \delta_{p6}, \quad \delta_{q3} = 2\delta_{q0} - \delta_{q6}. \end{cases} \tag{20}$$

Thus, it can be found that the power slopes of the reversed voltage vector pair are symmetrical with respect to the power slope of zero vector. If the selected vector is V_{n1}, its opposite vector is named as V_{-n1}, and the corresponding active and reactive power slope are δ_{-pn1} and δ_{-qn1}, respectively; it is same for V_{n2}. The power slope relation is derived as follows:

$$\begin{cases} \delta_{pn1} = 2\delta_{pz0} - \delta_{-pn1}, \ \delta_{qn1} = 2\delta_{qz0} - \delta_{-qn1} \\ \delta_{pn2} = 2\delta_{pz0} - \delta_{-pn2}, \ \delta_{qn2} = 2\delta_{qz0} - \delta_{-qn2}. \end{cases} \tag{21}$$

While the calculated duration based on (15) has negative value, for instance, t_1 is negative and t_2 is positive; by substituting δ_{pn1} and δ_{qn1} from (21) into (12), we have

$$\begin{cases} P_{err} = P^* - \left\{P^k + 2\left[(2\delta_{pz0} - \delta_{-pn1})t_1 + \delta_{pn2}t_2 + \delta_{pz0}t_0\right]\right\} \\ Q_{err} = Q^* - \left\{Q^k + 2\left[(2\delta_{qz0} - \delta_{-qn1})t_1 + \delta_{qn2}t_2 + \delta_{qz0}t_0\right]\right\}. \end{cases} \tag{22}$$

It can be rewritten as follows:

$$\begin{cases} P_{err} = P^* - \left\{P^k + 2\left[\delta_{-pn1}(-t_1) + \delta_{pn2}t_2 + \delta_{pz0}(t_0 + 2t_1)\right]\right\} \\ Q_{err} = Q^* - \left\{Q^k + 2\left[\delta_{-qn1}(-t_1) + \delta_{qn2}t_2 + \delta_{qz0}(t_0 + 2t_1)\right]\right\}. \end{cases} \tag{23}$$

TABLE III
VOLTAGE-VECTORS' SEQUENCES FOR RPDCC

Vector sequence	$t_1>0, t_2>0$	$t_1<0, t_2>0$	$t_1>0, t_2<0$	$t_1<0, t_2<0$
t_1'	t_1	$-t_1$	t_1	$-t_1$
t_2'	t_2	t_2	$-t_2$	$-t_2$
t_0'	t_0	t_0+2t_1	t_0+2t_2	$t_0+2t_1+2t_2$
V_{n1}'	V_{n1}	V_{-n1}	V_{n1}	V_{-n1}
V_{n2}'	V_{n2}	V_{n2}	V_{-n2}	V_{-n2}

Then, the duration could be correspondingly rescheduled as (24) to meet the dead-beat control performance

$$t_1' = -t_1, \quad t_2' = t_2, \text{ and } \quad t_0' = t_0 + 2t_1. \tag{24}$$

It means that the opposite vector V_{-n1} could be selected to replace V_{n1} to achieve the positive duration when $t_1 < 0$, and the corresponding duration is $-t_1$. Meanwhile, the duration time of zero vector is adjusted to be $t_0 + 2t_1$ to ensure the dead-beat control performance. The vector reselection and corresponding durations for all the conditions are presented in Table III, the duration of nonzero vectors remains its absolute value, and the duration of each vector still meets the following equation:

$$t_1' + t_2' + t_0' = T_s/2. \tag{25}$$

Thus, the calculation of t_0' can still be easily derived as in (26), and the dead-beat control performance is theoretically ensured.

$$t_0' = T_s/2 - |t_1| - |t_2|. \tag{26}$$

It should be noted that the negative duration of zero-vector would appear with a large power error, which is unavoidable with least-square optimization based duration calculation methods since the negative duration is also caused by external factors. In this case, the zero-vector duration will be forced to zero, and the duration of nonzero vectors will be adjusted in proportion to the abstract value of corresponding duration. Compared with the IPDCC method, there is no need to recalculate the power slopes of active and reactive powers, and the recalculation of durations using (15) is eliminated. Thus, the computation burden is reduced. Besides, both the negative duration issue of t_1 and t_2 can be solved, and the dynamic adjustment of V_{n1} and V_{n2} could further improve the steady and dynamic performance. The RPDCC is illustrated in Fig. 5.

B. Vector Sequence Arrangement and Switching Frequency Comparison

With consideration of minimizing jumps between each vector during implementation, the frequency reduction and lower switching loss can be achieved. For switching frequency reduction, there are mainly two aspects regarding vector sequence after vector selection of the proposed RPDCC method. The first one is selecting an appropriate zero vector to produce minimal switching jumps while switching between the nonzero vector and the zero vector. Another aspect is exchanging the sequence

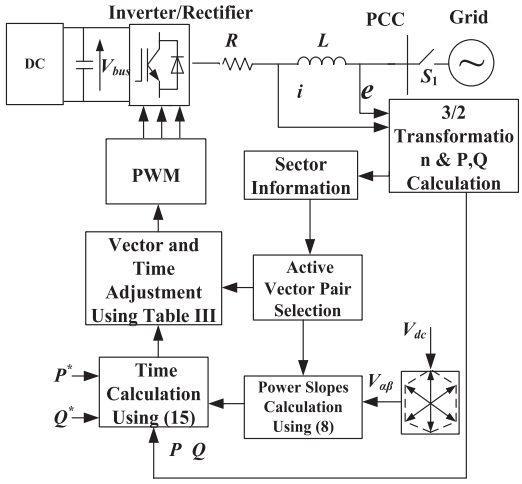

Fig. 5. Block diagram of the RPDCC for the ac/dc converter.

of two selected nonzero vector dynamically to achieve minimal jumps between previous vector sequences.

With these principles, the switching frequency comparison of each scheme is conducted. It should be noted that the comparison below is only under the condition of negative duration, since if there is no negative duration calculated, the vector sequence of IPDCC and RPDCC is the same as CPDCC. Taking sector II as an example, as seen from Fig. 6(a) and Fig. 6(b), the vector sequence of IPDCC has two switches within each control period T_s, which is same as CPDCC. In comparison, while there is one reverse vector replacement, as shown in Fig. 6(c) and Fig. 6(e), the vector sequence of RPDCC has only one more switch, namely three switches. As there are two nonzero reverse vector replacements under the condition of $t_1 < 0, t_2 < 0$, it has two switches as in Fig. 6(d). Though the comparison takes sector II as an example, the regularity of switch numbers in other sectors is the same. In conclusion, under the same sampling frequency, the IPDCC has almost the same switching frequency as CPDCC, which can be easily estimated by sampling frequency. The switching frequency of RPDCC would increase slightly since the phenomenon of negative duration only comprises a small proportion of the whole control period after RPDCC is applied, which can be verified by the simulations and experiments. In terms of switching between the original vector and the reversed vector, as shown in Fig. 6, the only difference of vector sequence between RPDCC with reversed voltage vector and the CPDCC is the additional one switch change in the vector sequence, which are quite common circumstances in STDPC methods [7]–[12], thus there is no compatible issue in RPDCC as well.

C. Design of One-step-delay Compensation

The influence of one-step-delay cannot be neglected for the proposed method. First, the converter voltage V is reconstructed from the applied active voltage vectors and corresponding duty ratio as

$$\bar{V} = V_{n1}' d_1' + V_{n2}' d_2' \tag{27}$$

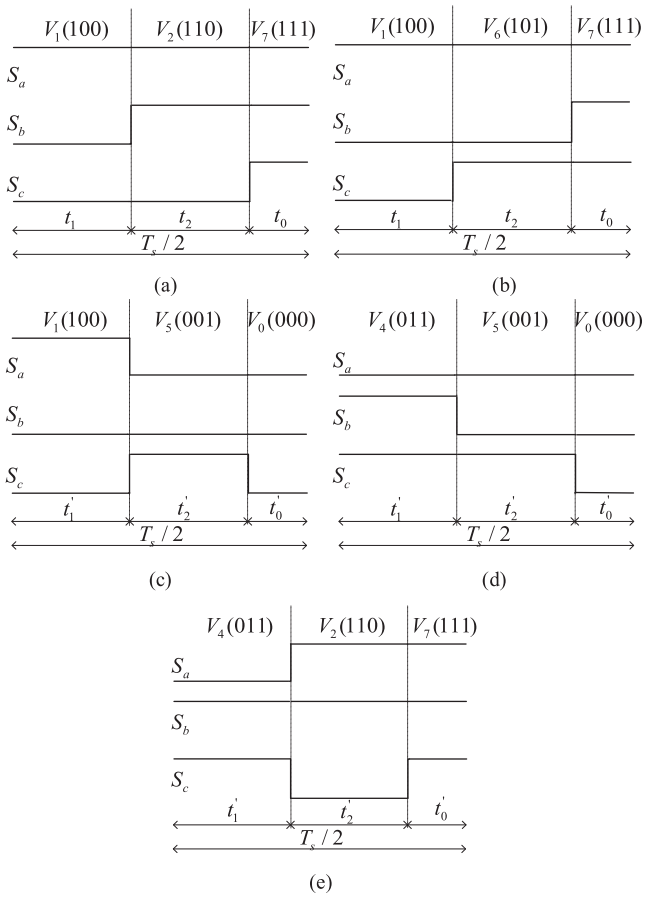

Fig. 6. Graphical diagram of different sequences. (a) CPDCC with sequence $(V_1V_2V_7)$. (b) IPDCC with sequence $(V_1V_6V_7)$. (c) RPDCC with sequence $(V_1V_5V_0)$ when $t_1 > 0,\ t_2 < 0$. (d) RPDCC with sequence $(V_4V_5V_0)$ when $t_1 < 0,\ t_2 < 0$. (e) RPDCC with sequence $(V_4V_2V_7)$ when $t_1 < 0,\ t_2 > 0$.

TABLE IV
ELECTRICAL PARAMETERS OF POWER CIRCUIT

Resistance of reactor	R	510 mΩ
Inductance of reactor	L	4 mH
DC-bus capacitor	C	680 uF
Load resistance	R_L	34 Ω
Source voltage	e	36 V(peak)
Source voltage frequency	f	50 Hz
DC-bus voltage	V_{dc}	120 V

where $d_1'=2t_1'/T_s$ and $d_2'=2t_2'/T_s$ are duty ratios of the selected two nonzero vectors. By substituting (27) into (10), the prediction value P^{k+1} and Q^{k+1} at the (k + 1)th instant can be obtained as

$$\begin{bmatrix} P^{k+1} \\ Q^{k+1} \end{bmatrix} = T_s \left(-\frac{R}{L} \begin{bmatrix} P^k \\ Q^k \end{bmatrix} + \omega \begin{bmatrix} -Q^k \\ P^k \end{bmatrix} \right) + \begin{bmatrix} P^k \\ Q^k \end{bmatrix} + \frac{3T_s}{2L} \begin{bmatrix} \left(|\bar{e}|^2 - \mathrm{Re}\left(\bar{e}\bar{V}^*\right) \right) \\ -\mathrm{Im}\left(\bar{e}\bar{V}^*\right) \end{bmatrix}. \quad (28)$$

Then, the values of P^{k+2} and Q^{k+2} can be calculated for each nonzero voltage vector with initial states of P^{k+1} and Q^{k+1}, and the equation for predicting P^{k+2} and Q^{k+2} is similar to (11), expressed as

$$\begin{cases} P^{k+2} = P^{k+1} + 2(\delta_{pn1}t_1 + \delta_{pn2}t_2 + \delta_{pz0}t_0) \\ Q^{k+2} = Q^{k+1} + 2(\delta_{qn1}t_1 + \delta_{qn2}t_2 + \delta_{qz0}t_0). \end{cases} \quad (29)$$

The cost function used to calculate the optimal duration could be revised

$$J = (P^* - P^{k+2})^2 + (Q^* - Q^{k+2})^2. \quad (30)$$

VI. SIMULATION RESULTS

The converter control with each control scheme has been numerically simulated using MATLAB/Simulink tool. The main electrical parameters used in the simulation are listed in Table IV. The compensation method proposed in Section IV is also applied for CPDCC and IPDCC in the following simulation and experiments. For convenience, the power flow from the ac power supply to the dc load is defined as positive. The sampling frequency keeps same as 20 kHz.

A. Steady-State Performance Comparison

To compare the steady-state performance, the ac three-phase input current and instantaneous active and reactive powers of the system are depicted; the nonzero vector pair selection and calculated duration are also presented. In Fig. 7, the active power reference keeps at 450 W and reactive power reference keeps at 0 Var. As seen from Fig. 7(a), the power ripples of both active and reactive powers are quite high with CPDCC, the *P* ripple is 19.82 W and *Q* ripple is 17.34 Var, and the power notches are quite serious. The current total harmonic distortion (THD) is as high as 6.46% due to current spikes. The nonzero vector pair selection is strictly selected according to sector information based on Table I with no adjustment at any circumstances, which results in the negative value of duration, the significant current notches, and active and reactive power pulsations. In comparison, with the complementary sequence Table II, IPDCC reselects the nonzero vector V_{n2} according to Table II when the calculated duration t_2 is negative with the selected vector pair based on Table I, while V_{n1} keeps unchanged at any time. Then, the durations of reselected vector pair are recalculated, which almost eliminates the negative value of t_2. Thus, it achieves much better results than CPDCC. The THD is significantly decreased to 2.26%, the *P* ripple is significantly reduced to 8.92 W, and *Q* ripple is only 5.51 Var, as shown in Fig. 7(b), which validates the superiority of IPDCC. However, as seen from the recalculated duration results t_1 and t_2 in Fig. 7(b), though after recalculation, t_1 and t_2 still have a large amount of negative value, especially of t_1, compensation measure is needed before actuation, which means the negative duration issue is not solved eventually and deteriorates the performance. In Fig. 7(b), the negative duration of t_1 appears a lot around 0.01 and 0.02 s, and the active and reactive power notches increase significantly compared with that at 0 s.

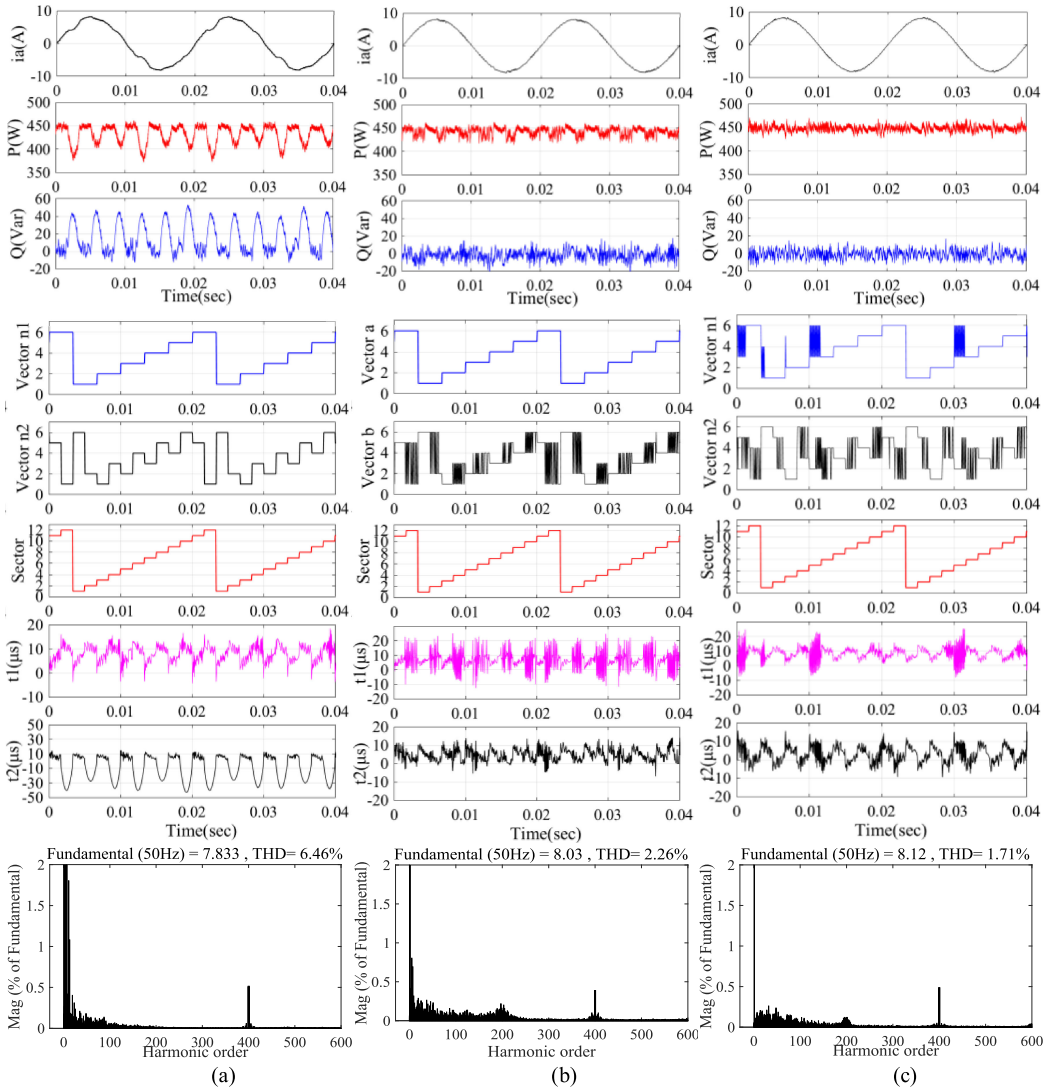

Fig. 7. Steady-state performance at $P = 450$ W, $Q = 0$ Var. Top to bottom: i_a, P and Q, V'_{n1}, V'_{n2}, sector, t_1,t_2, THD analyses of i_a. (a) CPDCC. (b) IPDCC. (c) RPDCC.

With the proposed RPDCC method, the steady performance is further improved without recalculation of duration, and the reverse vector of original selected vector based on Table I is selected whenever there exists a negative duration, thus both negative duration issues of V_{n1} and V_{n2} could be adjusted, as presented in Fig. 7(c). The current THD is further decreased to only 1.71% with RPDCC, and the current is more sinusoidal compared with the IPDCC. The active and reactive power ripples are further decreased to 6.06 W and 4.64 Var, respectively, and the power notches are almost eliminated.

In terms of switching frequency comparison, since the CPDCC and IPDCC have two switches of three-phase full-bridge in one control period as analyzed above, the averaged switching frequency f_s can be theoretically derived by $f_s = (2/3)/T_s$, which is 13.33 kHz. The measured average switching frequencies in the simulation at $P = 450$ W and $Q = 0$ Var are 13.3 kHz and 13.2 kHz for CPDCC and IPDCC, respectively, which is slightly lower than the theoretically calculated result, since there could be only one switch if the duration of the certain vector is forced to zero in the actuation. Meanwhile, the measured switching frequency of RPDCC is 15.1 kHz, which does not increase too much as expected due to fact that the lasting time of negative duration only comprises quite a small proportion of each control period after applying RPDCC as seen from Fig. 7(c). Also, it is concluded that the fixed switching frequency is achieved for each control scheme.

For bidirectional power flow comparison, the steady-state performance at $P = -350$ W and $Q = 200$ Var with each method is compared as seen from Fig. 8 and similar conclusions can be achieved, i.e., the switching frequency of the RPDCC is 14.1 kHz, which is slightly increased compared with that of CPDCC (12.5 kHz) and IPDCC (12.8 kHz). The quantitative comparison of steady-state performance including current THD, active and reactive power ripples is presented in Table V. Both the IPDCC and RPDCC methods improve the steady-state performance significantly in comparison with the CPDCC method, and the RPDCC has the best steady-state performance among the sector information based vector selection methods.

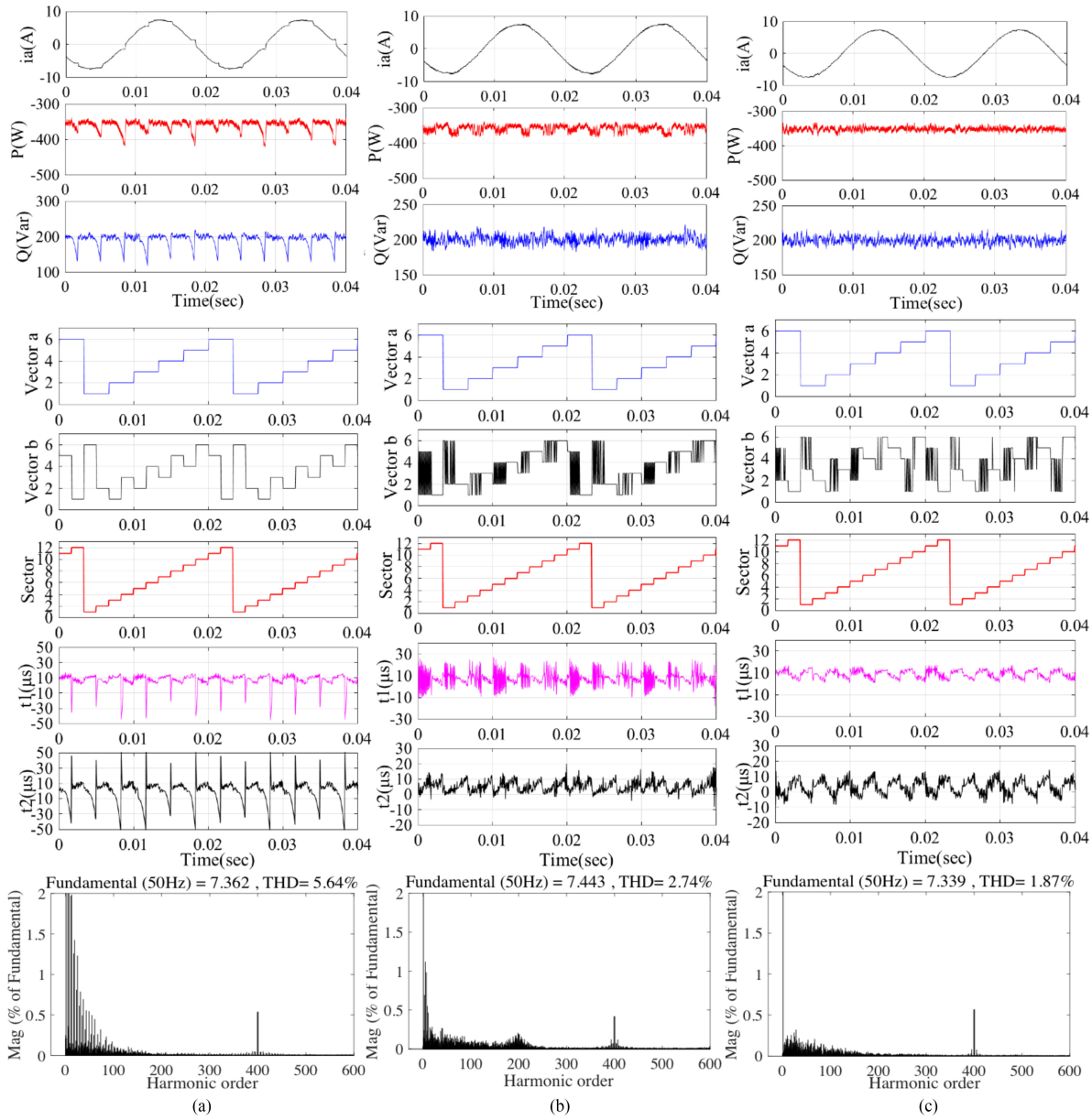

Fig. 8. Steady-state performance at $P = -350$ W, $Q = 200$ Var. Top to bottom: i_a, P and Q, V'_{n1}, V'_{n2}, sector, t_1, t_2, THD analyses of i_a. (a) CPDCC. (b) IPDCC. (c) RPDCC.

TABLE V
QUANTITATIVE COMPARISONS OF SIMULATION RESULTS [46]

Control method	*P=450 W Q=0 Var*			*P=-350 W Q=200 Var*			*Response (at 0.01 s)*	*Over shoot*	*Response (at 0.03 s)*	*Over shoot*
	THD(%)	*Prip* (W)	*Qrip*(Var)	*THD(%)*	*Prip* (W)	*Qrip* (Var)	*Time*(s)	*Q*(Var)	*Time*(s)	*P*(W)
CPDCC	6.46	19.82	17.34	5.64	14.2	17.05	0.001	25	0.0017	370
IPDCC	2.26	8.92	5.51	2.74	9.30	5.49	0.0012	79	0.0021	380
RPDCC	1.71	6.06	4.64	1.87	5.59	4.77	0.0002	22	0.0014	171
MPCDDC-I	1.64	5.36	4.87	1.72	4.62	5.18	0.0001	12	0.0018	147
MPCDDC-II	1.55	5.23	4.72	1.86	5.34	5.18	0.0001	13	0.0015	22
ISVMDPC	2.19	7.78	5.36	2.21	7.11	4.86	0.0007	29	0.0035	143
MPCPDCC-I	1.41	5.05	3.86	1.6	4.67	4.69	0.0001	13	0.0009	118
MPCPDCC-II	1.54	5.31	4.81	1.64	4.9	4.85	0.0001	18	0.0009	21
RMPCPDCC	1.55	5.59	4.41	1.77	4.96	5.03	0.0001	16	0.0009	119

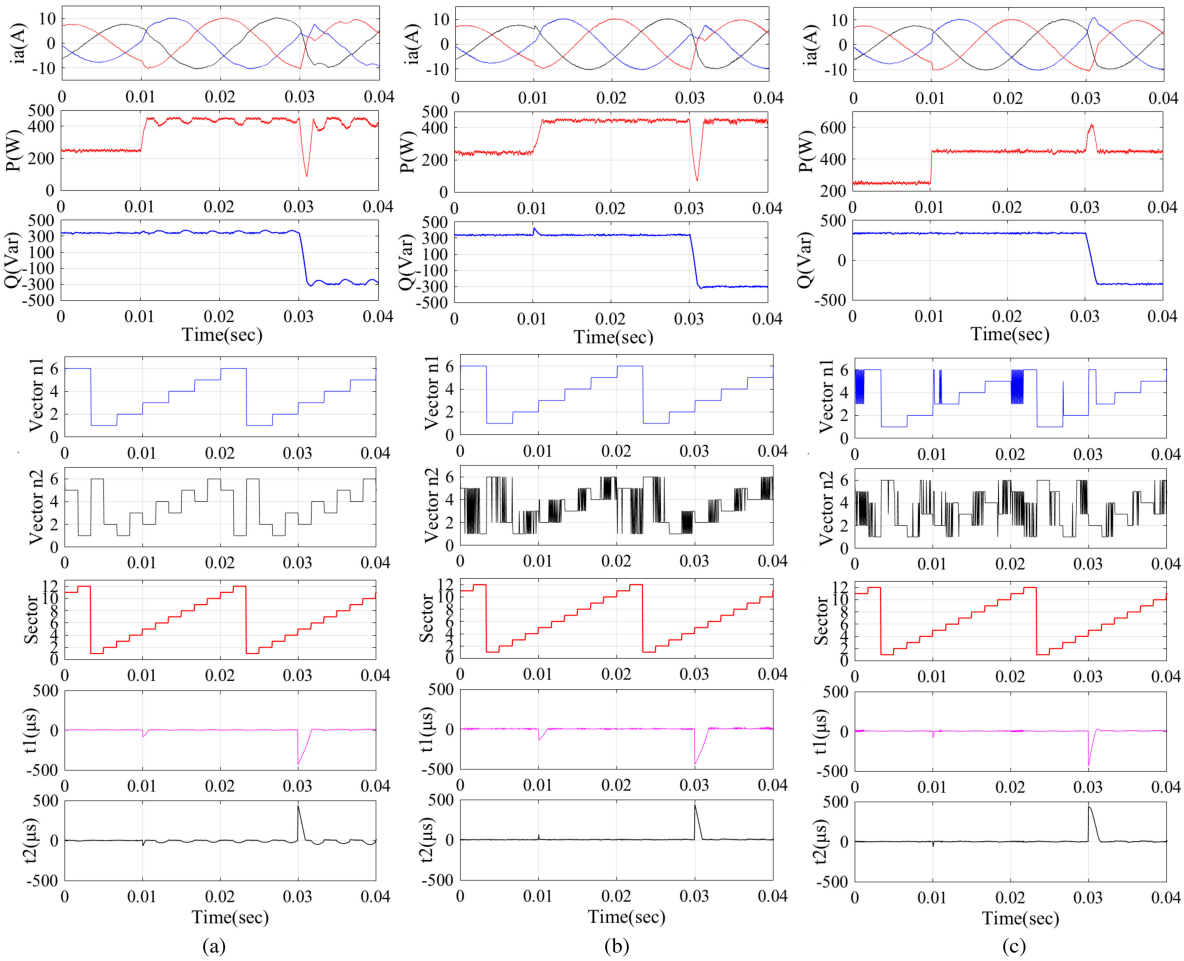

Fig. 9. Dynamic-state performance comparison. Top to bottom: i_a, P and Q, V'_{n1}, V'_{n2}, sector, t_1,t_2 (a) CPDCC. (b) IPDCC. (c) RPDCC.

The quantitative comparisons of steady-state performance with other related methods are presented in Table V as referenced from [46]. The model predictive control based duty cycle control (MPDCC) methods are two vector-based methods with model predictive cost function for vector selection. The improved space vector modulator based direct power control (ISVMDPC) as in [31] use the SVM module to generate the switching signals. The three vector-based methods with model predictive cost function for vector selection are denoted as MPCPDCC. It is concluded that the model predictive cost function based methods achieve much better steady-state performance compared with other categories. Due to page limitations and main targets of this paper, refer to [46] for more details about the comparisons.

B. Dynamic-State Performance Comparison

The transient responses of active and reactive power are shown in Fig. 9. The active power reference value steps up from 250 to 450 W at 0.01 s while the reactive power reference remains at 350 Var at the beginning and is changed to –300 Var at 0.03 s. The influence of δ_{qz0} on negative duration occurrence in Section IV can be verified. With the operating condition in Fig. 7, δ_{qz0} calculated by (8) is 0.14 Mvar/s, and the occurrence of negative duration is serious in Fig. 7(a); while before 0.01s in Fig. 9(a), the occurrence of negative duration is almost eliminated since δ_{qz0} is only 0.03 Mvar/s.

When P has the step change and instantaneous P_{err} increases as shown in Fig. 9(a), the nonzero vectors V_3 and V_2 are selected at 0.01 s with CPDCC. The corresponding calculated durations are both negative, which indicates the reverse vectors would be the optimal choice, but with CPDCC only zero vector is implemented for actuation. Thus, it reduces the adjustment efforts, and the response time is as high as 0.001s. With IPDCC as shown in Fig. 9(b), the nonzero vector selection is same as CPDCC since t_2 keeps positive, but V_3 is not implemented since t_1 keeps negative, and the reactive power overshoot is 79 Var. With RPDCC, the reverse vectors of V_3 and V_2 are selected once P_{err} increases according to the calculated negative duration and implemented in the whole adjustment period, which significantly decreases the response time to 0.0015 s and almost eliminate reactive power overshoot. Meanwhile, the P overshoot when Q has a step change is also reduced with RPDCC at 0.03 s in Fig. 9. The quantitative comparison of dynamic performance is presented in Table V.

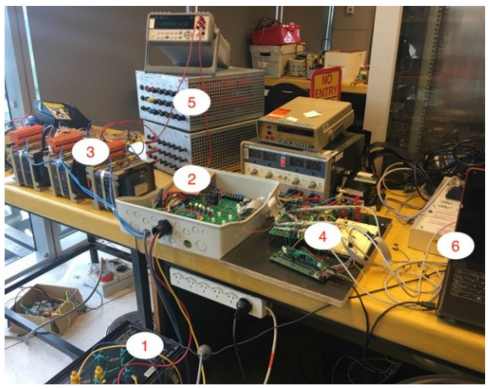

Fig. 10. Experimental setup of ac/dc converter. (1) Three-phase isolated transformer. (2) Three-phase ac/dc converter main circuit. (3) Inductors. (4) TI C2000 target board and interface board. (5) DC resistive load. (6) PC.

TABLE VI
ELECTRICAL PARAMETERS OF EXPERIMENTAL PROTOTYPE

Resistance of reactor	R	500 mΩ
Inductance of reactor	L	22 mH
DC-bus capacitor	C	680 uF
Load resistance	R_L	34 Ω
Source voltage	e	120 V
Sampling frequency	fs	10 kHz
Source voltage frequency	f	50 Hz

In conclusion, the proposed RPDCC is the best one among sector information based vector selection control methods in steady and dynamic performance. As shown in Table V, the RPDCC achieves the best comparison indicators. The quantitative comparisons of dynamic performance with other related methods are presented in Table V as [46]. It shows that the model predictive cost function based vector selection methods generally have ability to eliminate the power overshoot with additional constraint. Due to page limitations and main targets of this paper, refer to [46] for more details.

VII. EXPERIMENTAL RESULTS

A scale-down prototype is constructed, as shown in Fig. 10. The system parameters are presented in Table VI. The main three-phase full-bridge circuit was constructed with a Fuji intelligent IGBT power module 6MBP50RA. It was controlled by a TMS320F28335 floating-point digital signal processor (DSP) based on Texas Instruments (TI) C2000 target board for A/D sampling, PWM signal generation, and D/A output. The variables such as reference value changes are controlled using real-time data exchange communication between the DSP and PC.

A. Comparisons of Steady-State Performance

To compare the steady-state performance, the THD and the power ripple of active and reactive powers at steady state of different power levels have been measured and calculated with each control. The sampling frequency for each method keeps same with 10 kHz. Fig. 11 shows the input phase to phase voltage V_{ab}, V_{bc}, input current i_a and i_b of each control method at $P = 450\,\text{W}$, $Q = 0\,\text{Var}$. The detailed analyses have been presented based on the experimental data acquired from oscilloscope to PC, such as instant active power, reactive power, harmonic spectra analyses of current i_b, and average switching frequency.

The active and reactive powers track the reference value successfully with each control, whereas the steady-state performance varies significantly. With the CPDCC method, the P ripple is 36.88 W, the Q ripple is 38.03 Var, and the current THD is 7.67%, as shown in Fig. 11(a). The average switching frequency is also calculated based on the acquired data of PWM driving signal from DSP, which is 6.6 kHz. While the performance is much improved with the IPDCC as shown in Fig. 11(b), the power ripple and THD are decreased dramatically; the switching frequency is 6.7 kHz and keeps almost the same with CPDCC, which aligns well with the theoretical analyses. With the proposed RPDCC, the current THD is further decreased to 4.64%, the reactive power ripple is decreased obviously to 22.08 Var, whereas the switching frequency is slightly increased to 7.3 kHz. The steady-state performance at $P = 200\,\text{W}$, $Q = 350\,\text{Var}$ is also compared as shown in Fig. 12, and similar conclusions can be observed. The quantitative comparisons of each control method are presented in Table VII.

In order to investigate the complexity of each control algorithm, the computation time in DSP is measured by setting two break points between the initial and the end of interrupt service routine with Code Composer Studio software of TI. The results are presented in Table VII. The computation time of IPDCC is 71.3 μs, which increases significantly compared with that of RPDCC (43.5 μs) and CPDCC (47.6 μs). The less control complexity of RPDCC is verified compared with IPDCC. Since they are less than the sampling time, these controls can be implemented completely in each control period.

In conclusion, the RPDCC achieves better steady-state performance with lower power ripple and current harmonics than CPDCC and IPDCC, and the computational burden is decreased compared with IPDCC though the switching frequency is slightly increased, which verifies the theoretical analyses and simulation results well.

B. Comparison of Dynamic-State Performance

The dynamic performance of each method is also compared comprehensively with series of experimental results. The active power steps up from 250 to 450 W, while the reactive power keeps at 330 Var.

Fig. 13 shows the experimental results of dynamic performance for each control method. Each method tracks the reference value accurately during the dynamic instant. However, it is seen that the dynamic response is quite different. As shown in Fig. 13(a), the response time of CPDCC when P changes from 250 to 450 W is 0.0051 s, it decreases to 0.0015 s with IPDCC. With the proposed RPDCC method, it further decreases to only 0.0008 s, as can be seen from Fig. 13(c), the response time of each control is presented in Table VII, which

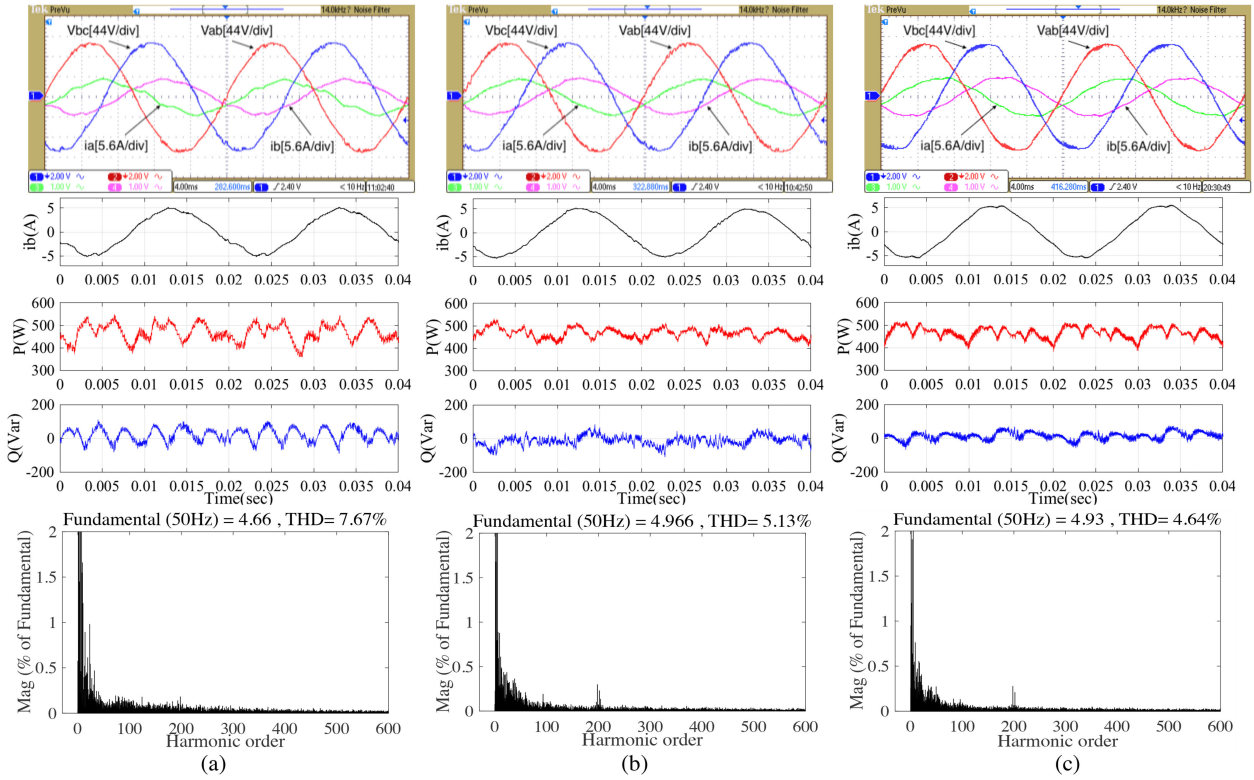

Fig. 11. Steady performance $P = 450\,\text{W}$, $Q = 0\,\text{Var}$. From top to bottom, experimental figure, i_b, P and Q, THD of i_b. (a) CPDCC. (b) IPDCC. (c) RPDCC.

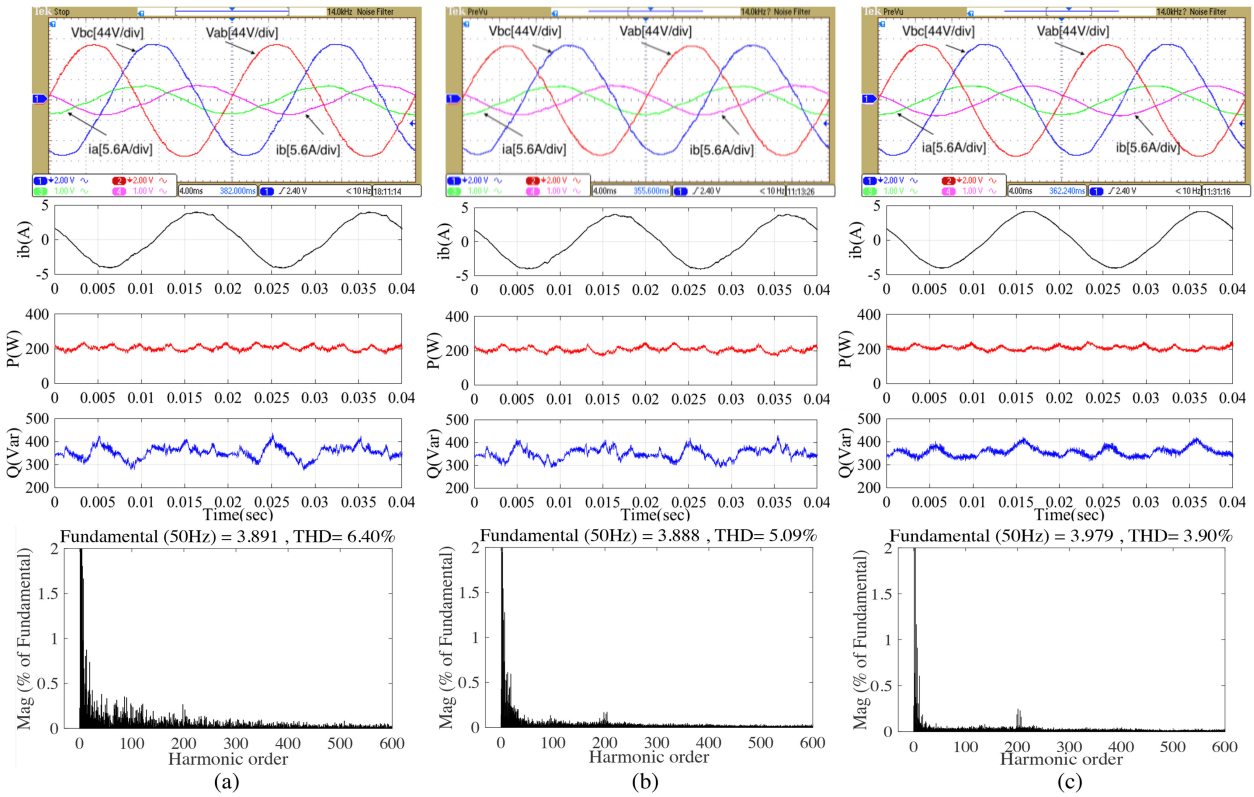

Fig. 12. Steady performance $P = 200\,\text{W}$, $Q = 350\,\text{Var}$. From top to bottom, experimental figure, i_b, P and Q, THD of i_b. (a) CPDCC. (b) IPDCC. (c) RPDCC.

TABLE VII
QUANTITATIVE COMPARISON OF EXPERIMENTAL RESULTS

Control	*P=450 W Q=0 Var*				*P=200 W Q=350 Var*				*Response*	*Computation*
	THD (%)	*Prip* (W)	*Qrip* (Var)	*fs* (kHz)	*THD* (%)	*Prip* (W)	*Qrip* (Var)	*fs* (kHz)	*Time* (s)	*Time* (μs)
CPDCC	7.67	36.88	38.03	6.6	6.4	16.99	28.94	6.6	0.0051	43.5
IPDCC	5.13	22.54	27.7	6.7	5.09	14.34	24.22	6.6	0.0015	71.3
RPDCC	4.64	24.86	22.08	7.3	3.9	12.08	19.57	7.1	0.0008	47.6

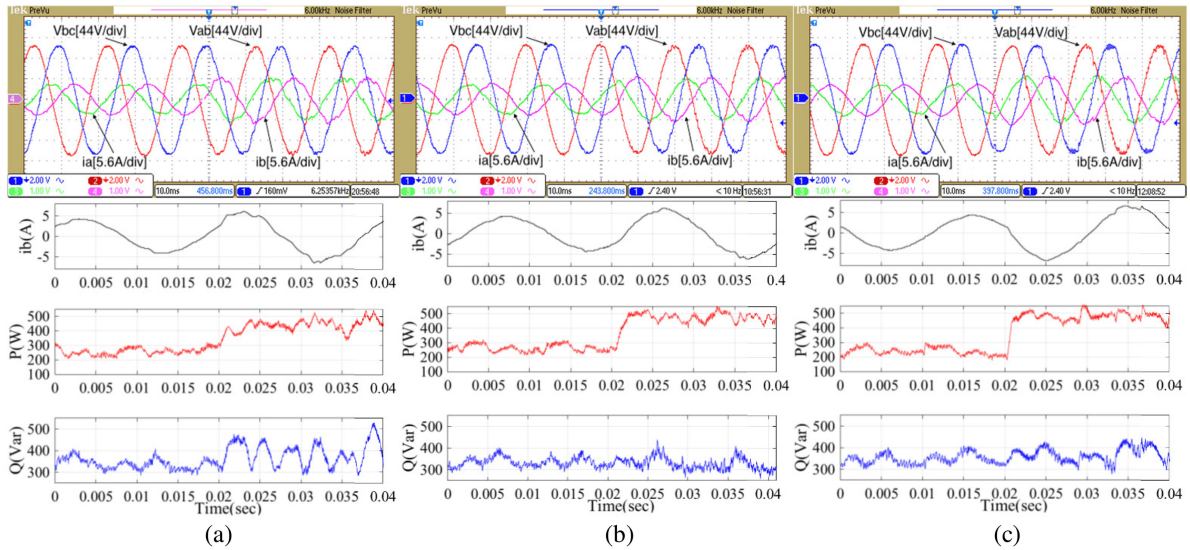

Fig. 13. Dynamic-state performance when P changes from 250 to 450 W, $Q = 330$ Var. Top: Experimental figure. Bottom: i_b, P and Q. (a) CPDCC. (b) IPDCC. (c) RPDCC.

TABLE VIII
COMPARATIVE RESULTS OF EACH CONTROL SCHEME

	CPDCC	IPDCC	RPDCC
Current harmonics	High	Medium	Low
Power ripples	High	Medium	Low
Algorithm/Calculation Complexity	Low	High	Low
Response time	High	Medium	Low
Switching frequency	Low	Low	Medium

verifies the fast dynamic response of RPDCC in comparison with IPDCC and RPDCC. It is due to the flexibility of implementing reversible dual nonzero vectors of RPDCC simultaneously whenever they have negative durations especially with the instantaneous large power error, while in comparison, the application of dual nonzero vectors is limited by negative durations with CPDCC and IPDCC. Finally, the comparative summary of each control method is depicted in Table VIII, which verifies the superiority of RPDCC.

C. System Parameter Redundancy

The robustness of RPDDC is examined when the line inductance is different from its real value. The inductance value used in the control with 50% to 200% of the real value (20 mH) is applied for comparison. As shown in Fig. 14(a), if 10 mH is used, the ripple of active power increases and the positive dc offset in the reactive power appears. If the inductance value increases to 30 and 40 mH, there is a slight influence on the reactive power ripple, and positive dc offset in the active power

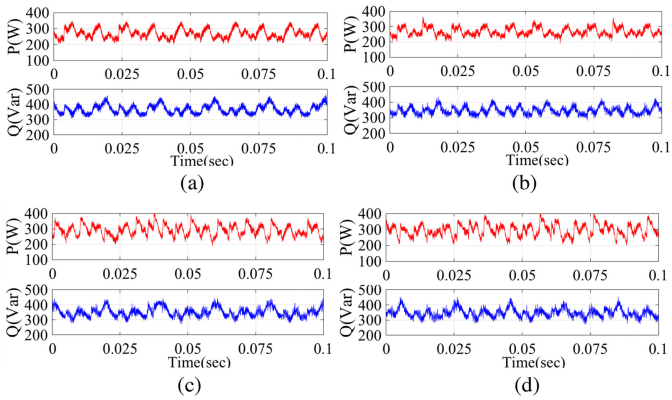

Fig. 14. Responses of active power and reactive power for proposed RPDDC when the actual inductance in control differs from the real value. (a) 10 mH. (b) 20 mH. (c) 30 mH. (d) 40 mH.

appears, as in Fig. 14(c) and (d). The results indicate that accuracy of inductance has a slight influence on the steady-state performance as the system stability is not influenced in the range of $-50\%-100\%$ inductance variations.

VIII. CONCLUSION

This paper proposes the RPDCC of three-phase ac/dc converters with improved control performance and reduced computational burden. First, the principle of CPDCC is presented, the reasoning of negative duration is comprehensively analyzed,

which is not only in relation with the selected vectors but also with the instantaneous power error and control period. Then, the drawbacks of IPDCC and its unsolved issue are fully discussed, including of high-control complexity, lacking selection flexibility of V_{n1}, losing sight of the negative value of t_1 and adjustment to avoid deterioration on control performance. Finally, the RPDCC is proposed to solve these issues. The principles of vector pair selection, theoretical derivation of duration calculation, switching frequency comparison, and control delay compensation are discussed in detail. The complementary vector sequence table and recalculation of durations are eliminated compared with IPDCC.

Simulation and experimental results are presented to compare the performance of each control scheme. The results verify the superior dynamic and steady-states performance of the proposed RPDCC method. The reason of better performance is discussed in detail, which aligns well with the theoretical analyses. In conclusion, while the IPDCC method improves the steady-state performance by reducing power ripple and current harmonics in comparison with the CPDCC method, the proposed RPDCC could solve the negative duration issue fundamentally and achieve even better steady-state performance with lower computation burden, though the switching frequency is slightly increased. In terms of the dynamic performance, the RPDCC method achieves faster response time and less power overshoot compared with the CPDCC and IPDCC methods.

REFERENCES

[1] J. R. Rodriguez, J. W. Dixon, J. R. Espinoza, J. Pontt, and P. Lezana, "PWM regenerative rectifiers: State of the art," *IEEE Trans. Ind. Electron.*, vol. 52, no. 1, pp. 5–22, Feb. 2005.

[2] L. Moran, M. Diaz, V. Higuera, R. Wallace, and J. Dixon, "A three-phase active power filter operating with fixed switching frequency for reactive power, current harmonic compensation," in *Proc. IEEE Trans. Ind. Electron.*, 1992, pp. 362–367.

[3] S. Chakraborty, B. Kramer, and B. Kroposki, "A review of power electronics interfaces for distributed energy systems toward achieving low-cost modular design," *Renew. Sustain. Energy Rev.*, vol. 13, no. 9, pp. 2323–2335, 2009.

[4] E. C. Santos, C. B. Jacobina, E. R. Silva, and N. Rocha, "Single-phase to three-phase power converters: State of the art," *IEEE Trans. Ind. Electron*, vol. 27, no. 5, pp. 2437–2452, May 2012.

[5] N. Flourentzou, V. G. Agelidis, and G. D. Demetriades, "VSC-based HVDC power transmission systems: An overview," *IEEE Trans. Power Electron.*, vol. 24, no. 3, pp. 592–602, Mar. 2009.

[6] Y. Zhang, Z. Li, Y. Zhang, W. Xie, Z. Piao, and C. Hu, "Performance improvement of direct power control of PWM rectifier with simple calculation," *IEEE Trans. Power Electron.*, vol. 28, no. 7, pp. 3428–3437, Jul. 2013.

[7] J. Hu, J. Zhu, and Dorrell, "In-depth study of direct power control strategies for power converters," *IET Power Electron.*, vol. 7, no. 7, pp. 1810–1820, Jul. 2014.

[8] J. Alonso-Martinez, J. E. Carrasco, and S. Arnaltes, "Table-based direct power control: A critical review for microgrid applications," *IEEE Trans. Power Electron.*, vol. 25, no. 12, pp. 2949–2961, Dec. 2010.

[9] B. Chen and G. Joos, "Direct power control of active filters with averaged switching frequency regulation," *IEEE Trans. Power Electron.*, vol. 23, no. 6, pp. 2729–2737, Nov. 2008.

[10] L. Xu, D. Zhi, and L. Yao, "Direct power control of grid connected voltage source converters," in *Proc. IEEE Power Eng. Soc. Gen. Meet.*, 2007, pp. 1–6.

[11] T. Noguchi, H. Tomiki, S. Kondo, and I. Takahashi, "Direct power control of PWM converter without power-source voltage sensors," *IEEE Trans. Ind. Appl.*, vol. 34, no. 3, pp. 473–479, May/Jun. 1998.

[12] P. Cortes, J. Rodriguez, P. Antoniewicz, and M. P. Kazmierkowski, "Direct power control of an AFE using predictive control," *IEEE Trans. Power Electron.*, vol. 23, no. 5, pp. 2516–2523, Sep. 2008.

[13] D. Zhi, L. Xu, and B.W. Williams, "Improved direct power control of grid-connected DC/AC converters," *IEEE Trans. Power Electron.*, vol. 24, no. 5, pp. 1280–1292, May 2009.

[14] S. Aurtenechea, M. A. Rodriguez, E. Oyarbide, and J. R. Torrealday, "Predictive control strategy for DC/AC converters based on direct power control," *IEEE Trans. Ind. Electron.*, vol. 54, no. 3, pp. 1261–1271, Jun. 2007.

[15] A. Sato and T. Noguchi, "Voltage-source PWM rectifier-inverter based on direct power control and its operation characteristics," *IEEE Trans. Power Electron.*, vol. 26, no. 5, pp. 1559–1567, May 2011.

[16] P. Cortes, M. Kazmierkowski, R. Kennel, D. Quevedo, and J. Rodriguez, "Predictive control in power electronics and drives," *IEEE Trans. Ind. Electron.*, vol. 55, no. 12, pp. 4312–4324, Dec. 2008.

[17] Bouafia, F. Krim, and J. P. Gaubert, "Fuzzy-logic-based switching state selection for direct power control of three-phase PWM rectifier," *IEEE Trans. Ind. Electron.*, vol. 56, no. 6, pp. 1984–1992, Jun. 2009.

[18] J. Restrepo, J. Viola, J. M. Aller, and A. Bueno, "A simple switch selection state for SVM direct power control," in *Proc. IEEE Int. Symp.Ind. Electron.*, Montreal, QC, Canada, Jul. 2006, vol. 2, pp. 1112–1116.

[19] J. Hu, L. Shang, Y. He, and Z. Q. Zhu, "Direct active and reactive power regulation of grid-connected dc/ac converters using sliding mode control approach," *IEEE Trans. Power Electron.*, vol. 26, no. 1, pp. 210–222, Jan. 2011.

[20] S. Vazquez, J. A. Sanchez, J. M. Carrasco, J. I. Leon, and E. Galvan, "A model-based direct power control for three-phase power converters," *IEEE Trans. Ind. Electron.*, vol. 55, no. 4, pp. 1647–1657, Apr. 2008.

[21] P. Antoniewicz and M. P. Kazmierkowski, "Virtual flux predictive direct power control of three phase AC/DC converter," in *Proc. Human Syst. Interact.*, 2008, pp. 510–515.

[22] S. Vazquez *et al.*, "Model predictive control: A review of its applications in power electronics," *IEEE Ind. Electron. Mag.*, vol. 8, no. 1, pp. 16–31, Mar. 2014.

[23] C. Xia, T. Liu, T. Shi, and Z. Song, "A simplified finite-control-set model-predictive control for power converters," *IEEE Trans. Ind. Informat.*, vol. 10, no. 2, pp. 991–1002, May 2014.

[24] R. Aguilera, P. Lezana, and D. Quevedo, "Finite-control-set model predictive control with improved steady-state performance," *IEEE Trans. Ind. Informat.*, vol. 9, no. 2, pp. 658–667, May 2013.

[25] S. Kwak, U.-C. Moon, and J.-C. Park, "Predictive-control-based direct power control with an adaptive parameter identification technique for improved AFE performance," *IEEE Trans. Power Electron.*, vol. 29, no. 11, pp. 6178–6187, Nov. 2014.

[26] J. Rodriguez *et al.*, "State of the art of finite control set model predictive control in power electronics," *IEEE Trans. Ind. Informat.*, vol. 9, no. 2, pp. 1003–1016, May 2013.

[27] J. Hu, J. Zhu, G. Platt, and D. G. Dorrell, "Multi-objective model-predictive control for high power converters," *IEEE Trans. Energy Convers.*, vol. 28, no. 3, pp. 652–663, Sep. 2013.

[28] D. E. Quevedo, R. P. Aguilera, M. A. Perez, P. Cortes, and R. Lizana, "Model predictive control of an AFE rectifier with dynamic references," *IEEE Trans. Power Electron.*, vol. 27, no. 7, pp. 3128–3136, Jul. 2012.

[29] P. Cortes, J. Rodriguez, C. Silva, and A. Flores, "Delay compensation in model predictive current control of a three-phase inverter," *IEEE Trans. Ind. Electron.*, vol. 59, no. 2, pp. 1323–1325, Feb. 2012.

[30] S. Kouro, P. Cortes, R. Vargas, U. Ammann, and J. Rodriguez, "Model predictive control-a simple and powerful method to control power converters," *IEEE Trans. Ind. Electron.*, vol. 56, no. 6, pp. 1826–1838, Jun. 2009.

[31] A. Bouafia, J.-P. Gaubert, and F. Krim, "Predictive direct power control of three-phase pulse width modulation (PWM) rectifier using space-vector modulation (SVM)," *IEEE Trans. Power Electron.*, vol. 25, no. 1, pp. 228–236, Jan. 2010.

[32] R. Portillo, S. Vazquez, J. I. Leon, M. M. Prats, and L. G. Franquelo, "Model based adaptive direct power control for three-level NPC converters," *IEEE Trans. Ind. Informat.*, vol. 9, no. 2, pp. 1148–1157, May 2013.

[33] S. Kwak and J.-C. Park, "Switching strategy based on model predictive control of VSI to obtain high efficiency and balanced loss distribution," *IEEE Trans. Power Electron.*, vol. 29, no. 9, pp. 4551–4567, Sep. 2014.

[34] S. Aurtenechea, M. A. Rodriguez, E. Oyarbide, and J. R. Torrealday, "Predictive control strategy for DC/AC converters based on direct power control," *IEEE Trans. Ind. Electron.*, vol. 54, no. 3, pp. 1261–1271, Jun. 2007.
[35] P. Antoniewicz and M. P. Kazmierkowski, "Virtual-flux-based predictive direct power control of AC/DC converters with online inductance estimation," *IEEE Trans. Ind. Electron*, vol. 55, no. 12, pp. 4381–4390, Dec. 2008.
[36] R. P. Aguilera, D. E. Quevedo, S. Vazquez, and L. G. Franquelo, "Generalized predictive direct power control for AC/DC converters," in *Proc. ECCE Asia*, Jun. 2013, pp. 1215–1220.
[37] J. Hu and Z. Q. Zhu, "Investigation on switching patterns of direct power control strategies for grid-connected DC–AC converters based on power variation rates," *IEEE Trans. Power Electron.*, vol. 26, no. 12, pp. 3582–3598, Dec. 2011.
[38] J. Hu and Z. Zhu, "Improved voltage-vector sequences on dead-beat predictive direct power control of reversible three-phase grid-connected voltage-sourced converters," *IEEE Trans. Power Electron.*, vol. 28, no. 1, pp. 254–267, Jan. 2013.
[39] Z. Song, W. Chen, and C. Xia, "Predictive direct power control for three-phase grid-connected converters without sector information and voltage vector selection," *IEEE Trans. Power Electron.*, vol. 29, no. 10, pp. 5518–5531, Oct. 2014.
[40] Z. Song, Y. Tian, W. Chen, Z. Zou, and Z. Chen, "Predictive duty cycle control of three-phase active-front-end rectifiers," *IEEE Trans. Power Electron.*, vol. 31, no. 1, pp. 698–710, Jan. 2016.
[41] Y. Zhang, Y. Peng, and H. Yang, "Performance improvement of two-vectors-based model predictive control of PWM rectifier," *IEEE Trans. Power Electron.*, vol. 31, no. 8, pp. 6016–6030, Aug. 2016.
[42] D. Choi and K. Lee, "Dynamic performance improvement of AC/DC converter using model predictive direct power control with finite control set, " *IEEE Trans. Ind. Electron.*, vol. 62, pp. 757–767, Feb. 2015.
[43] Y. Zhang, W. Xie, Z. Li, and Y. Zhang, "Low-complexity model predictive power control: Double-vector-based approach," *IEEE Trans. Ind. Electron.*, vol. 61, no. 11, pp. 5871–5880, Nov. 2014.
[44] Y. Zhang and Y. Peng, "Model predictive current control with optimal duty cycle for three-phase AC/DC converters," in *Proc. IEEE Int. Power Electron. Appl. Conf. Expo.*, 2014, pp. 837–842.
[45] Y. Zhang, W. Xie, Z. Li, and Y. Zhang, "Model predictive direct power control of a PWM rectifier with duty cycle optimization," *IEEE Trans. Power Electron.*, vol. 28, no. 11, pp. 5343–5351, Nov. 2013.
[46] X. Shi, "Advanced control of three-phase full-bridge converter in microgrids," Ph.D. dissertation, Dept. Elect. Data Eng., Univ. Technol. Sydney, Australia, 2017.

Xiaolong Shi (S'13) received the B.E. and the M.E. degrees from Beijing Jiaotong University, Beijing, China, in 2011 and 2014, respectively, both in electrical engineering. From 2017, he is working toward the Ph.D. degree at the University of Technology Sydney, Sydney, Australia.

He is currently with the School of Data and Electrical Engineering, University of Technology Sydney, Sydney, NSW, Australia. His research interests include design, optimization, and advanced control algorithms of power converters and renewable energy systems.

Jianguo Zhu (S'93–M'96–SM'03) received the B.E. degree from the Jiangsu Institute of Technology, Jiangsu, China, in 1982, the M.E. degree from the Shanghai University of Technology, Shanghai, China, in 1987, and the Ph.D. degree from the University of Technology Sydney (UTS), Sydney, Australia, in 1995, all in electrical engineering. He worked as a Lecturer with UTS in 1994 and a Full Professor in 2004 and Distinguished Professor of electrical engineering in 2017. In 2018, he joined the University of Sydney, Camperdown, Australia, as a Full Professor and the Head of School, School of Electrical and Information Engineering. His research interests include computational electromagnetics, measurement and modeling of magnetic properties of materials, electrical machines and drives, power electronics, renewable energy systems, and smart microgrids.

Li Li received the B.S. degree from the Huazhong University of Science and Technology, Wuhan, China, in 1996, the M.S. degree from Tsinghua University, Beijing, China, in 1999, and the Ph.D. degree from the University of California, Los Angeles, CA, USA, in 2005.

From 2005 to 2007, he was a Research Associate with the University of New South Wales, Australian Defence Force Academy (UNSW@ADFA). From 2007 to 2011, he was a Researcher at the National ICT Australia, Victoria Research Laboratory, Department of Electrical and Electronic Engineering, The University of Melbourne. In 2011, he joined UTS, where he is currently an Associate Professor. His research interests include control theory and power system control.

Dr. Li held several visiting positions at the Beijing Institute of Technology, Tsinghua University, and UNSW@ADFA. He is presently serving as an Associate Editor of *IET Renewable Power Generation*.

Dylan Dah-Chuan Lu (M'04–SM'09) received the B.E. and Ph.D. degrees from The Hong Kong Polytechnic University, Hong Kong, in 1999 and 2004, respectively.

In 2003, he joined PowereLab Ltd. as a Senior Design Engineer and was responsible for industrial switching power supply projects. From 2006 to 2016, he was a Full-Time Faculty Member with The University of Sydney. He currently holds an Honorary position at the University of Sydney, Sydney, Australia. Since July 2016, he has been working as an Associate Professor with the School of Electrical and Data Engineering, University of Technology Sydney, Australia. His current research interests include efficient and reliable power conversion for renewable sources, energy storage systems, and microgrids.

Dr. Lu was the recipient of the 2015 Best Paper Award in the category of Emerging Power Electronic Technique at the IEEE PEDS. He presently serves as an Associate Editor of the IEEE TRANSACTIONS ON CIRCUITS AND SYSTEMS II and a Subject Editor of the *IET Renewable Power Generation*. He is a member of Engineers Australia.

Jianwei Zhang received the bachelor's degree in electrical engineering from the Northwest A&F University, Xianyang, China, in 2014. Since then, he has been working toward the Ph.D. degree in electrical engineering at the University of Technology Sydney (UTS), Sydney, Australia.

From 2015, he has been working as a Casual Academic at the Faculty of Engineering and IT, UTS. His research interests include control of power electronic converters, matrix converters, microgrids, and ac motor drives.

Haitao Yang (S'16) received the B.S. degree from the Hefei University of Technology, Hefei, China, in 2009, and the M.S. degree from the North China University of Technology, Beijing, China, in 2015, both in electrical engineering. He is currently working toward the Ph.D. degree in mechanical engineering at the School of Mechanical and Mechatronic Engineering, University of Technology Sydney, Sydney, Australia. His research interests include motor drives, position/speed sensorless control of ac motors, PWM converters, and electric vehicles.